JOURNAL OF MATERIALS SCIENCE 29 (1994) 5441–5448

Effect of zinc and iron on the (micro-)structure and copper charge excess of the YBaCuO superconductor

A. LANCKBEEN, P. H. DUVIGNEAUD*, P. DIKO, M. MEHBOD, G. NAESSEN*, R. DELTOUR
*Université Libre de Bruxelles, B-1050 Bruxelles, Belgium Service de Physique des Solides C.P.233, and *Service de Chimie Industrielle et Analytique C.P.165,*

Samples of $YBa_2(Cu_{1-y}Zn_y)_3O_{7-y}$ and $YBa_2(Cu_{1-y}Fe_y)_3O_{7+x}$, with y in the range 0.0–0.16 for zinc and 0.0–0.30 for iron were synthesized by solid-state reaction. The solubility limit has been found to be equal to 7% and 19 at % for zinc and iron, respectively. Zinc has little effect on the structure which remains orthorhombic throughout all the zinc concentration range, while iron induces an important structural modification (tweed structure formation). Both impurities induce grain-growth inhibition but densification appears to be independent of the impurity content with respect to the undoped material. However, iodometry shows that the oxygen stoichiometry decreases in zinc-doped samples while it increases in iron-doped samples. Charge balance resulting from the dopant charge and the evolution of the copper charge with doping have been invoked. In zinc-doped samples, the copper charge excess (copper charge fraction > 2) decreases sharply for $0.0 \leqslant y < 0.04$, then it shows a plateau-like behaviour for $0.04 \leqslant y < 0.06$, while in iron-doped samples, it decreases almost monotonically. Confirming some of our previous results there is a correlated T_c decrease in the case of zinc-doped samples (occurrence of a T_c plateau) and in the case of iron-doped samples (quasi monotonical decrease). This difference has been interpreted in terms of structural changes related to the different substitution behaviour of zinc and iron.

1. Introduction

The double interest of a systematic study of doping by 3d impurities on the copper-sites of the ceramic superconductor $YBa_2Cu_3O_{7-x}$ (also called the 123 phase) lies, on the one hand, in an investigation method of the mechanism responsible for high-T_c superconductivity in this system and, on the other hand, in the study and the modification of its electrical current transport properties.

Among the various dopants usually substituted for copper, two of them have retained our attention: a non-magnetic (zinc) and a magnetic (iron) impurity. It is known that zinc [1–8] which does not have a magnetic moment causes, for example, a more rapid decrease of T_c (10 K/at %) than ions iron [4, 5, 7, 9, 10] (2 K/at %). Until now, this rather unexpected result was far from being completely clarified. In most interpretations, the inner structure of YBaCuO is involved, especially the type of copper site occupancy.

Many authors claim that the iron ions occupy selectively the Cu(1) chain sites (3, 5, 6, 11–16] while the zinc ions occupy the Cu(2) plane sites [2, 3, 5, 17–19]. However, there are many contradictory arguments in the literature for zinc [4, 20–23] and iron [5, 9, 20, 24] to occupy both Cu(1) and Cu(2) sites.

It is clear that beside the nature and content of the dopant, the preparation method and the related phase homogeneity, oxygen stoichiometry and copper site occupancy play an important role in the superconducting properties [4, 11, 25] and explain the scattering of the experimental results. For example, the limits of solubility of iron and zinc in the $YBa_2Cu_3O_{7-x}$ are not clearly stated, because the values in the literature vary in the range 15 %–22 % for iron [2, 5, 7, 9] and 7 %–12 % [2, 3, 5, 26] for zinc. Therefore, we have focused our work on the synthesis of high-homogeneity pure and doped materials and their careful chemical characterization.

By a global and systematic approach, this work aimed to determine the solubility limit of these impurities and to study their influence on the microstructure, oxygen content and critical temperature. The results are discussed in relation to microstructural changes and changes in the copper charge excess.

2. Experimental procedure

Samples of $YBa_2(Cu_{1-y}M_y)_3O_{7-x}$, $y_{nominal}$ ranging from $y_{nom} = 0.0$–0.16 for zinc and $y_{nom} = 0.0$–0.30 for iron, were synthesized from reagent-grade Y_2O_3, $BaCO_3$, CuO, ZnO or Fe_2O_3 by solid-state reaction.

The preparation method includes at least two thermal treatments at temperatures ranging from 905–

0022–2461 © *1994 Chapman & Hall*

950 °C in flowing oxygen with intermediate grinding in a planetary micromill and sieving ($\leqslant 25$ μm). After the last thermal treatment, the samples were cooled at 30 °C h^{-1} and were submitted to further oxygenation at 500 °C for 72 h.

The raw materials were mixed for 2 h in polyethylene jars containing ZrO_2 balls in an aqueous medium. The mean grain size was reduced to 0.5 μm.

The progressive rise in temperature of the thermal treatments was aimed at remaining at any step of the synthesis below the melting temperature of any composition from the $YO_{1.5}$–BaO–CuO phase diagram which can generate phase heterogeneities.

The preparation methods are referred to as methods I, II and III and correspond to thermal treatments at 905 and 930 °C for method I, at 905, 930 and 950 °C for method II and 924, 936, 948 °C for method III (the temperatures are given with an accuracy of $\pm$ 2 °C).

Samples were checked for homogeneity by X-ray diffraction after each thermal treatment, for grain-size distribution by laser granulometry and for grinding contamination by X-ray fluorescence. The grinding contamination was found to be lower than the purity grade of the reactants i.e. < 2000 p.p.m.

The microstructure of the samples was studied by optical microscopy in natural and polarized light and by scanning electron microscopy in relation to doping.

Electron microscope studies were carried out using a Jeol JSM-35c scanning electron microscope equipped with an energy dispersive X-ray microanalyser (EDAX). The phase compositional analysis was performed using the matrix correction program "ZAF". The oxygen stoichiometry was determined iodometrically. The two steps giving the Cu^{3+} content were carried out by potentiometric titration using an automatic titrator. On the other hand, a thermogravimetric method (TGA) based on copper reduction in flowing Ar–7% H_2 gas at 950 °C was applied.

The determination of the cell parameters of the doped samples was performed with a Siemens D 5000 X-ray diffractometer using CuK_α radiation and Rietveld refinement (DBWS 9006 (Young)).

3. Results

3.1. Microstructure and phase composition

In zinc-doped samples, nominal compositions y_{nom} = 0.0, 0.02, 0.04, 0.06 and 0.08 are monophasic by X-ray diffraction. Secondary phases such as CuO, $BaCuO_2$ and ZnO are detected in the sample of composition $y_{nom} = 0.16$.

SEM and EDAX studies show that in the concentration range y_{nom} = 0.0–0.08, CuO and $BaCuO_2$ are the two main secondary phases. Their content grows from 0.1% ($y_{nom} = 0.0$) to 0.5 vol % ($y_{nom} = 0.08$). The nature of those phases changes as the zinc nominal content is increased from $y_{nom} = 0.0$ to $y_{nom} = 0.16$, because CuO progressively decreases with concomitant increase of ZnO grains, attesting the reaching of the solubility limit of zinc in the 123 superconducting phase. On the basis of EDX measurements, the solubility limit of zinc in the 123 superconducting phase is estimated at $y_{123} = 0.07$ (Fig. 1).

The microstructure of zinc-doped samples reflects a good and homogeneous oxygenation, whatever the dopant concentration because twins, also characteristic of their orthorhombic structure, are present throughout all the samples (Fig. 2). In addition, the pores are homogeneously distributed in the samples and are located mainly at the grain boundaries. The porosity, which is nearly equal to 20 % in all compositions, is thus open and independent of the zinc content. However, pore and grain sizes decrease as a function of the zinc content. It is clear, by looking at Figs 2 and 5a below, representing, respectively, an $YBa_2(Cu_{0.92}Zn_{0.08})_3O_{6.89}$ sample and an $YBa_2Cu_3O_{6.93}$ sample at the same magnification (× 800), that zinc incorporation in the YBaCuO grains results in grain growth inhibition.

In iron-doped samples, compositions with y_{nom} = 0.02, 0.04, 0.08 and 0.16 and monophasic by XRD. EDAX analysis in the YBaCuO grains shows quantitative agreement with the nominal compositions of the above four samples. For $y_{nom} \leqslant 0.16$, the two main secondary phases are again CuO and $BaCuO_2$. Their content is always less than 0.5 vol %.

In the sample with $y_{nom} = 0.30$, a multiphase microstructure was observed (Fig. 3). Besides YBa_2

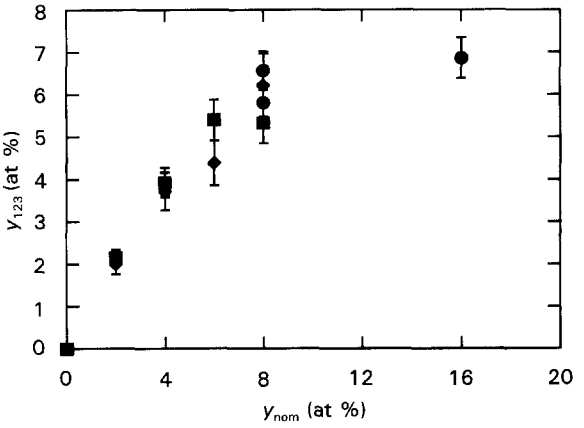

Figure 1 Zinc concentration in the 123 phase, y_{123} (y = Zn/Zn + Cu in at %), as a function of the zinc nominal content, $y_{nominal}$. (◆) Method I, (■) method II, (●) method III.

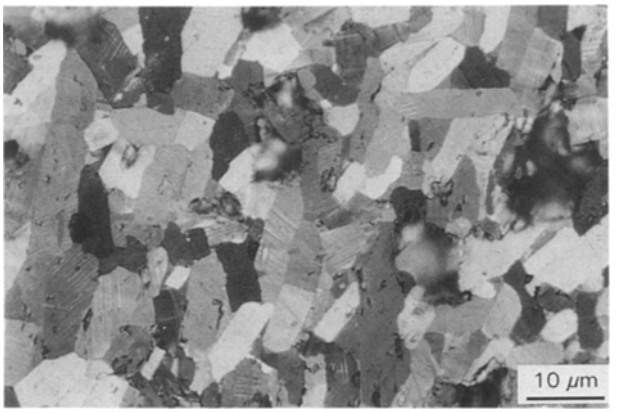

Figure 2 Optical micrograph in polarized light of an $YBa_2(Cu_{0.92}Zn_{0.08})_3O_{6.89}$ sample. Twins contrast.

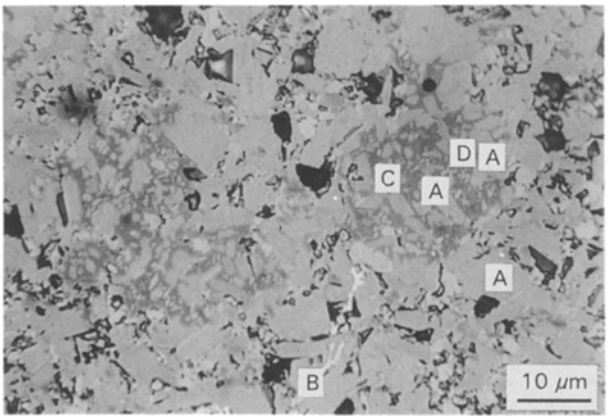

Figure 3 Optical micrograph in polarized light of an $YBa_2(Cu_{0.70}Fe_{0.30})_3O_{7+x}$ sample. Phase composition. A, $YBa_2(Cu_{1-y}Fe_y)_3O_{7+x}$; B, CuO; C, $YBaCuFeO_5$; D, Ba(CuFe) matrix.

$(Cu_{1-y}Fe_y)_3O_{7+x}$ grains, CuO, $BaCuO_2$ and YBa $CuFeO_5$ (the 1 1 1 1 phase) were found by XRD and by EDAX microanalysis. The secondary phases formed a separate structural component in which the $YBa_2(Cu_{1-y}Fe_y)_3O_{7+x}$ and $YBaCuFeO_5$ phases are embedded in a $Ba(CuFe)O_2$ matrix. In this matrix, the $YBaCuFeO_5$ phase crystallizes as flat ellipsoids. The maximum iron concentration in the $YBa_2(Cu_{1-y}Fe_y)_3O_{7+x}$ grains was estimated to be $y_{123} = 0.19$, which is considered here to be the solubility limit for iron (Fig. 4).

Iron-doped samples show the typical twinned orthorhombic to tweed pseudo-tetragonal structural transition.

Optimal contrast conditions were obtained by combining crossed or partially crossed polarizers with Laves–Ernst compensators. Whereas the undoped samples have strong twin contrast (Fig. 5a), this contrast is much weaker in the sample with $y_{123} = 0.02$ (Fig. 5b). In the samples with $y_{123} > 0.02$, the $YBa_2(Cu_{1-y}Fe_y)_3O_{7+x}$ grains are not twinned. From this concentration, a pseudo-tetragonal (orthorhombic) tweed structure is expected. This structure is formed by perpendicularly oriented very fine twin

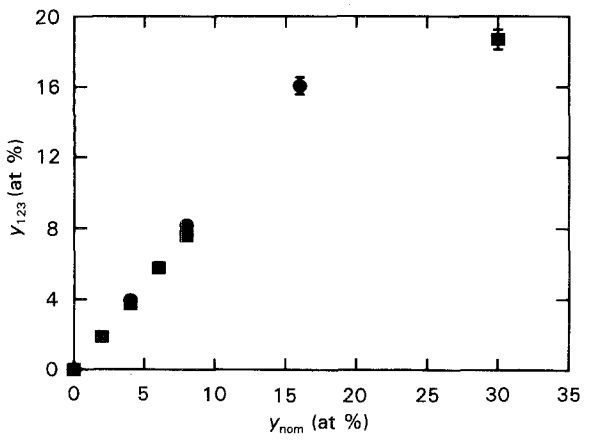

Figure 4 Iron concentration in the 123 phase, y_{123} (y = Fe/Fe + Cu in at %), as a function of the iron nominal content, $y_{nominal}$. (■) Method II, (●) method III.

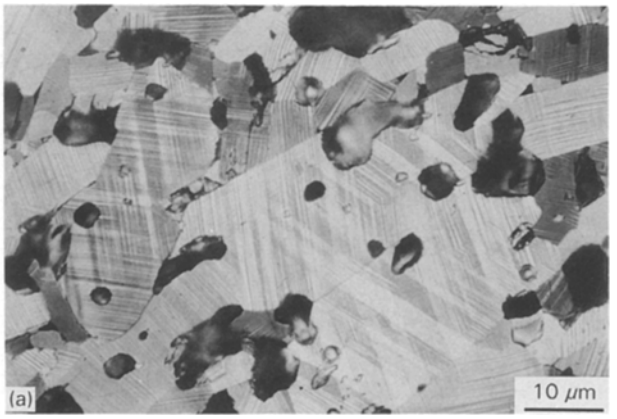

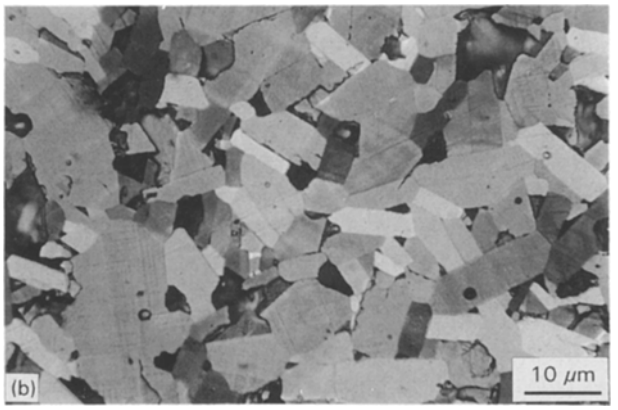

Figure 5 Optical micrographs in polarized light of (a) an $YBa_2Cu_3O_{6.93}$ sample, and (b) an $YBa_2(Cu_{0.98}Fe_{0.02})_3O_{6.96}$ sample. Twins contrast.

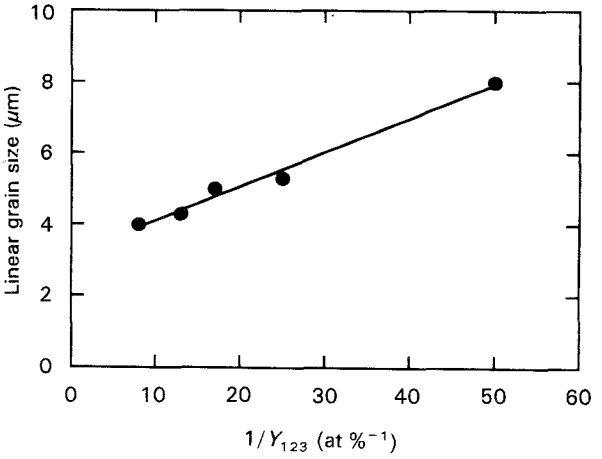

Figure 6 Linear grain-size evolution as a function of $1/y_{123}$, the inverse of the 123 phase iron content.

domains (< 10 nm) evinced by high-resolution electron microscopy (HREM), appearing tetragonal under X-ray diffraction. Such a fine microstructural element is well within the resolution limit of optical microscopy.

Here too, the porosity of the samples is practically independent of the iron content up to saturation and reaches 20%. The number of pores per square millimetre increases with the iron content. Besides, the iron dopant also plays the role of a grain-growth inhibitor (Fig. 6). The grain size diminution is particularly strong for $0.0 \leqslant y_{123} \leqslant 0.04$.

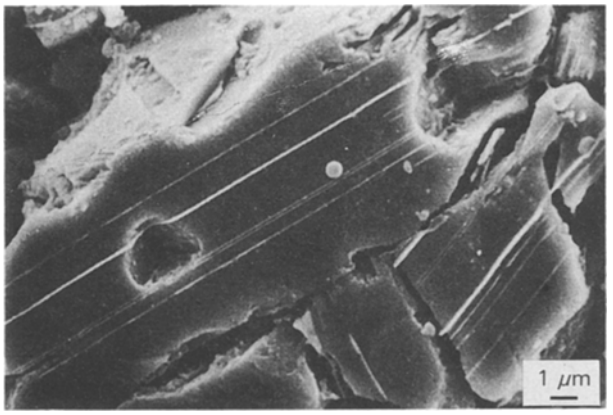

Figure 7 Scanning electron micrograph of *ab*-plane linear defects in an $YBa_2(Cu_{0.84}Fe_{0.16})_3O_{7+x}$ sample.

Furthermore, planar defects parallel to the "*ab*" plane were revealed by etching in the samples with $y_{123} = 0.076, 0.16$ and 0.19 (Fig. 7) in a 1 vol % bromine in ethanol solution. Their amount increases with the iron content in the $YBa_2(Cu_{1-y}Fe_y)_3O_{7+x}$ phase. Attempts to estimate their elemental composition by SEM-coupled EDAX microanalysis failed, owing to their thinness (< 0.1 μm). However, HREM studies revealed that these defects are iron clusters extending in one of the two [1 1 0] directions of the CuO chains (0 0 1) plane and that they are separated by about 30 *c* parameters [27].

3.2. Oxygen stoichiometry

Related oxygen stoichiometry determinations by iodometry and by TGA revealed that zinc has only a slight effect on the oxygen content of the samples. In fact, a slight decrease in oxygen stoichiometry from 6.93 (undoped) to 6.89 (saturated with zinc) occurs (Fig. 8).

In Fig. 9, the Cu^{3+} evolution with doping is expressed in terms of formal replacements of Cu^{2+} and Cu^{3+} by Zn^{2+}. The position of the experimental line in Fig. 9 indicates that the Cu^{3+} mol number decreases when the zinc concentration increases, but the formal Cu^{3+}:Cu^{2+} substitution ratio depends on the

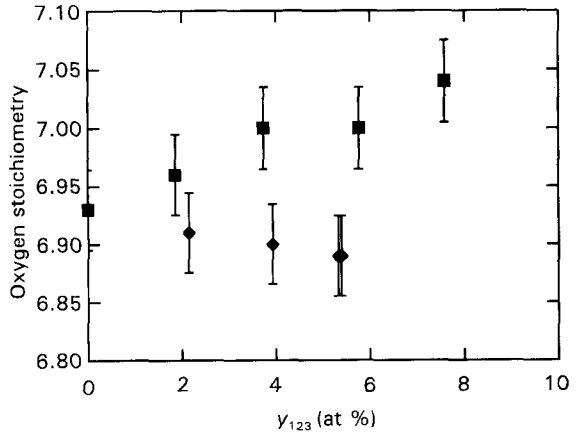

Figure 8 Oxygen stoichiometry as a function of y_{123}, the 123 phase dopant content ((◆) zinc or (■) iron).

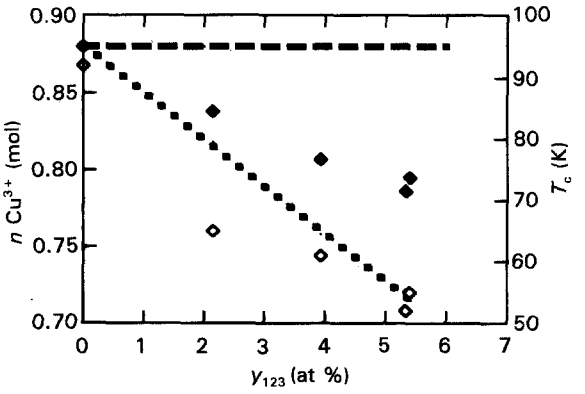

Figure 9 Cu^{3+} mole number per formula unit as a function of y_{123}, the 123 phase zinc content. Comparison between experimental and simulated values. (◆ ◆ ◆) Zn^{2+} replaces Cu^{3+}, (- - -) Zn^{2+} replaces Cu^{2+}, (◆) experimental values, (◇) critical temperature, T_c, evolution as a function of y_{123}.

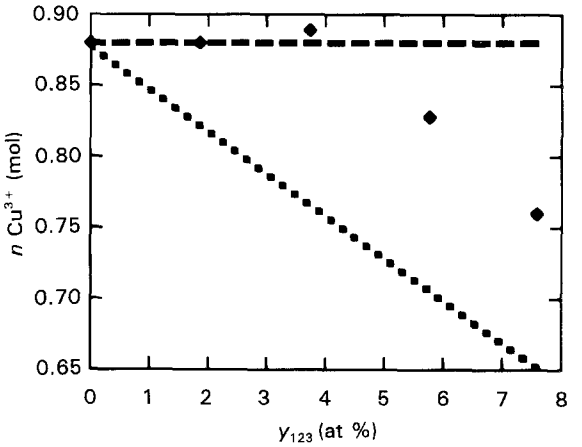

Figure 10 Cu^{3+} mole number per formula unit as a function of y_{123}, the 123 phase iron content. Comparison between experimental and simulated values. (◆ ◆ ◆) Fe^{3+} replaces Cu^{3+}, (- - -) Fe^{3+} replaces Cu^{2+}, (◆) experimental values.

zinc content (Cu^{3+}:Cu^{2+} = 2:1 for $y_{123} = 0.02$, 1:1 for $y_{123} = 0.054$). The average copper charge, calculated from the Cu^{2+} and Cu^{3+} mol numbers, ranges from $+2.32$ ($y_{123} = 0.0$), to $+2.26$ ($y_{123} = 0.02$), then $+2.23$ ($y_{123} = 0.04$) and $+2.22$ ($y_{123} = 0.054$). The charge fraction superior to $+2$ is referred to here as the copper charge excess, responsible for the superconducting properties of YBaCuO.

TGA curves emphasize the tendency towards oxygen stoichiometry lower than 7. However, imprecisions related to the zinc vapourization above 900 °C make iodometry a more suitable method for determining the oxygen stoichiometry in zinc-doped samples. In iron-doped samples, an increase in oxygen stoichiometry from 6.93 to 7.04 ($y = 0.076$) occurs (Fig. 8).

Comparison with simulations (Fig. 10) shows that the Cu^{3+} mol number remains unaffected for $0.0 \leqslant y_{123} \leqslant 0.04$. It decreases for $y_{123} > 0.04$ and the Cu^{3+}:Cu^{2+} formal substitution ratio reaches a 1:1 value for $y_{123} = 0.076$. However, the average copper charge, calculated from the Cu^{2+} and Cu^{3+} mol numbers, decreases from $+2.32$ ($y = 0.0$), to $+2.24$ ($y_{123} = 0.02$), then $+2.16$ ($y_{123} = 0.04$) and $+2.05$

($y_{123} = 0.057$), before reaching values inferior to +2 for $y_{123} > 0.08$, showing a disappearance of the copper charge excess. Thus values derived from TGA curves emphasize the tendency towards oxygen stoichiometry higher than 7. However, the equilibria are not easily reached owing to chemical reactions occurring between reduced iron oxide and barium oxide which make iodometry a more suitable oxygen stoichiometry determination method in this case too.

3.3. Lattice parameters

The lattice parameters were determined in fully oxygenated zinc- and iron-doped samples up to saturation. The results confirm the already observed [5, 6, 20, 26] maintenance of orthorhombicity in presence of zinc (Fig. 11). Minor changes are observed in the orthorhombic distortion ($b - a/b + a = 8.34 \times 10^{-3}$ for $y_{123} = 0.0$ and 8.45×10^{-3} for $y_{123} = 0.054$). The slight increase of a and b parameters and the nearly unchanged values of the c parameter result in a linear increase of the cell volume (Fig. 11).

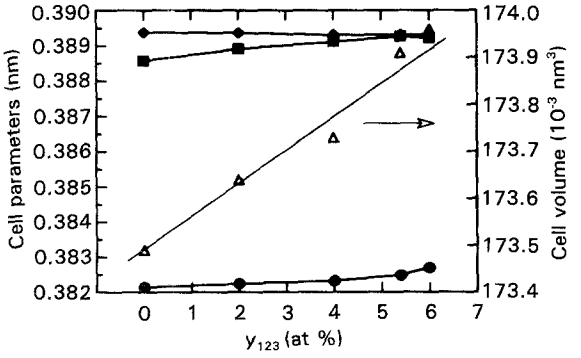

Figure 11 Lattice parameters (●) a, (■) b, (◆) $c/3$, and (△) cell volume evolutions as a function of y_{123}, the 123 phase zinc content.

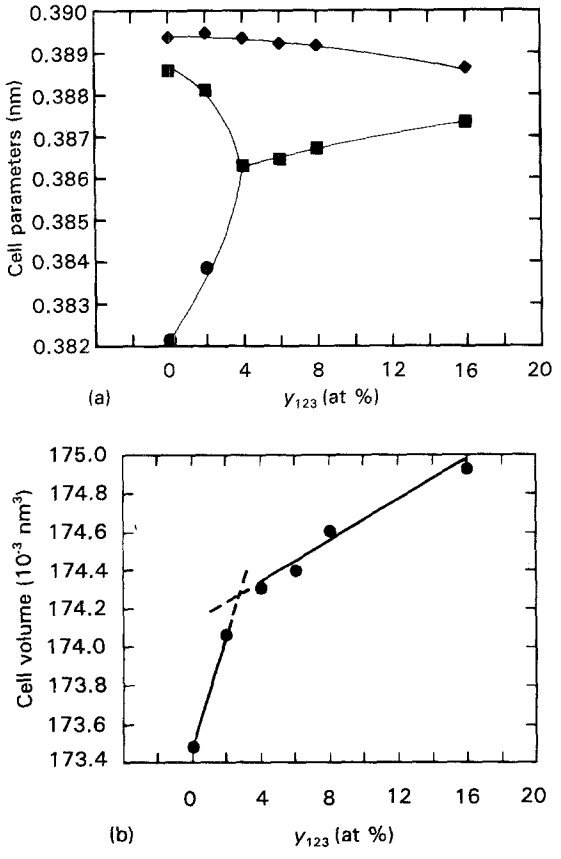

Figure 12 (a) Lattice parameters (●) a, (■) b, (◆) $c/3$, and (b) cell volume evolutions as a function of y_{123}, the 123 phase iron content.

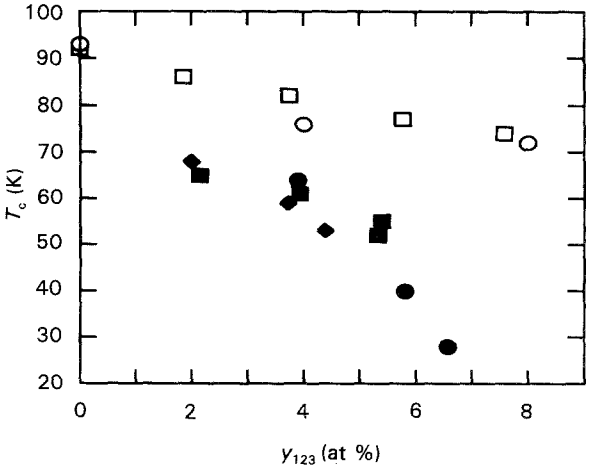

Figure 13 Critical temperature, T_c, as function of y_{123}, the 123 phase dopant content (Zn or Fe). (◆) Zn(method I) (■) Zn(method II), (●) Zn(method III), (□) Fe(method II), (○) Fe(method III).

In iron-doped samples (Fig. 12), the orthorhombic-pseudo tetragonal transition is completed for $y_{123} = 0.04$ [2, 5, 9, 15, 20, 28]. Up to this value, the increase of the cell volume is stronger than that in zinc-doped samples. Beyond $y_{123} = 0.04$, the increase of a and the decrease of c parameters result in a slower increase of the cell volume (Fig. 12).

3.4. Electrical properties

The T_c versus zinc doping curve shows a sharp decrease of T_c between $y_{123} = 0.0$ and 0.04 followed by a slower decrease up to $y_{123} = 0.054$ as previously reported [5, 8, 20] and then again by a sharper increase until saturation of the 123 phase is reached (Fig. 13). Note that T_c is rather insensitive to the thermal history because samples prepared by Methods I, II and III and containing the same amount of zinc (e.g. $y_{123} = 0.04$) have the same T_c (60 ± 3 K).

The T_c versus iron doping curve (Fig. 13) decreases more slightly and more monotonically than in zinc-doped samples, in a consistent way with the literature data [5, 9, 10].

4. Discussion

Zinc has little or no effect on the structure of YBaCuO because the lattice parameters only show a weak evolution. The orthorhombicity remains almost unchanged and twins are visible whatever the dopant concentration.

Iron has a much more pronounced effect on the structure as shown by the evolution of the lattice parameters (Fig. 12). The cell symmetry of the iron-doped samples changes from orthorhombic to pseudo-tetragonal between $y_{123} = 0.03$ and 0.04 and then

becomes tetragonal for $y_{123} = 0.057$ [27]. This evolution is related to the development of the tweed structure [29]. Before becoming equal, the a cell parameter increases more than the b parameter decreases, presumably because additional oxygen atoms necessary to balance the + 3 charge of iron are located on the usually empty O(5) position along the a axis [30].

The densification of YBaCuO at 950 °C in oxygen is found to be independent of the zinc and iron contents at concentrations lower than saturation, where sintering is likely to occur by a solid-state process. In this case, the sintering rate is controlled by the slowest species which are known to be yttrium and barium. Thus, this argument may explain why the atoms substituting for copper do not modify the densification of YBaCuO. As a consequence, all samples are oxygenated in the same manner, so that a comparison of the specific effects of the dopants is valid over a large concentration range. In contrast, the zinc and iron incorporation results in limiting the grain and pore sizes. This observation tends to indicate the absence of melting due to the presence of these impurities and confirms a solid-state mechanism for sintering. In the ceramic materials, grain-growth inhibition is often correlated with solute segregation at the grain interfaces due to elastic driving forces resulting from ionic radii differences and/or electrostatic driving forces resulting from valency differences and space charge effects [31]. The solute segregations at the grain boundaries could also be accounted for in iron-doped samples by the fact that iron may cluster in the Cu(1) plane at high doping levels. There is now evidence that iron can form rows along the [1 1 0] directions separated by orthorhombic domains [11]. These rows have indeed been evinced by HREM studies in our $y_{123} = 0.076$, 0.16 and 0.19 samples.

Oxygen stoichiometry can be used as a tool for the interpretation of electrical properties such as T_c because, in the YBaCuO crystalline structure, oxygen ions balance the cationic charges in order to match crystal electroneutrality requirements. In fact, in YBaCuO, the oxygen stoichiometry determines the copper charge excess evolution and the amount of charge transfer between copper chains (charge carriers reservoir) and copper planes (superconducting planes). Both quantities are closely related to the T_c value [32, 33]. These observations will be used here for doped systems in order to characterize the effect of zinc and iron doping on T_c.

It is very important to use iodometric titration in addition to TGA measurements when interpretating oxygen stoichiometry-related data in doped YBaCuO samples. TGA measurements allow a direct measurement of the sample's global oxygen content, but in doped samples, vapourization of the impurity, as in zinc-doped samples, or side reactions, as in iron-doped samples, add imprecisions to the measurements. Iodometry then proves to be very useful because it avoids these problems and gives direct access to the copper charge by measuring the Cu^{3+} and Cu^{2+} amount in the sample.

TGA measurements and iodometric titration show that the oxygen stoichiometry decreases in zinc-doped YBaCuO as the zinc content increases in agreement with a charge balance resulting from a decrease of the copper charge. On the other hand, in iron-doped samples, oxygen stoichiometry increases in agreement with the charge balance of the + 3 charge of iron, resulting in the incorporation of half an extra oxygen atom per iron atom in the structure.

Let us focus on the zinc-doped samples. The copper charge excess clearly shows a decrease mimicking the shape of the T_c versus zinc concentration curve (Fig. 13) for the same zinc concentration range ($0.0 \leqslant y_{123} \leqslant 0.054$). Because the global oxygen content remains almost unchanged by the doping and zinc induces a decrease of the copper charge excess, its effect on T_c is rather to be interpreted in terms of a charge carriers decrease on copper than in terms of an oxygen depletion consequence. For $0.0 \leqslant y \leqslant 0.04$, the dramatic T_c drop can be interpreted as an effect of zinc substituted in the CuO_2, which induces local magnetic moments [18] having a pair-breaking effect [34]. The subsequent sharp T_c drop for $y_{123} > 0.054$ observed in Fig. 13 can be viewed as a zinc detrimental effect on the charge transfer between chains and planes. Indeed, by substituting for copper in the chains, in addition to the planes, as evinced by oxygen isotherms point defects model [35], $Zn^{2+}(3d^{10})$ ions act as "insulating islands" interrupting the chains. As long as the average distance between two neighbouring Zn^{2+} ions in the chains ($0.02 \leqslant y_{123} \leqslant 0.054$) exceeds the length (8 or 9 copper atoms [33]) for efficient chain-to-plane charge transfer to occur, T_c is only slightly affected by the fraction of zinc substituted in the chains. When $y_{123} > 0.054$, this distance becomes inferior to the critical length and T_c again falls more sharply due to carriers localization on chain copper ions following this chains' length shortening.

The T_c plateau observed for $0.04 \leqslant y \leqslant 0.054$ is probably due to a non-linear charge transfer associated with the presence of zinc in the chains, as suggested elsewhere [35]. This interpretation contrasts with the usual assumptions about the effect of zinc on superconducting properties such as T_c, related to its localization in the YBaCuO crystalline structure, because it is assumed that zinc has a mixed copper-site occupancy instead of an exclusive Cu(2) site localization. It should be pointed out that these latter studies [2, 3, 5, 17–19] rely on neutron diffraction results and that among them, mixed copper-site occupancies are also found [36, 37]. These discrepancies are probably due to the fact that the scattering factors of copper and zinc are very close. On the other hand, several other experiments implying different techniques such as differential anomalous X-ray scattering [6], nuclear magnetic resonance [21], cluster calculations [22], point defects model [35] support a mixed copper-site occupancy picture and correlate very well.

These experiments interpret the change in the superconducting behaviour of YBaCuO as a consequence of the alteration of the role of the chains as carriers reservoir. The particular shape of the T_c versus zinc concentration curve (Fig. 13) observed in our experiments would then be the sum of the two mentioned

zinc effects dominating different parts of the zinc concentration range.

Let us now turn to the iron-doped samples. T_c also decreases according to the copper charge excess evolution, showing a slight discontinuity for $0.04 < y_{123} < 0.057$. This phenomenon could be due either to the structural changes caused by the iron substitution in the chains or by a change in the copper sites repartition occurring for $y_{123} > 0.04$. In the first case, our data suggest that as long as the material remains orthorhombic ($y_{123} \leqslant 0.04$), the chain length is still long enough to provide an efficient chain-to-plane charge transfer. When the material truly becomes tetragonal ($y_{123} > 0.04$), due to random distribution of the oxygen atoms in the Cu–O basal plane, the chain length is no longer long enough to provide the correct charge transfer. As a consequence, the charge transfer decreases due to carrier localization on the chains copper ions accompanied by a steeper T_c decrease and suppression of the superconducting transition before the saturation limit is reached.

In the second case, the change of iron repartition between the copper-sites in favour of Cu(2) would cause more iron to enter the CuO_2 planes and its effect to be a pair-breaking effect, due to its magnetic moment, leading to the suppression of the superconducting transition for $y_{123} > 0.076$. Indeed, recent neutron diffraction studies on isotope-substituted $YBa_2Cu_{2.76}Fe_{0.24}O_{7+x}$ [24] have shown that iron can have a 1:1 Cu(1):Cu(2) occupancy. However, the discontinuity in the Cu^{3+} mol number, copper charge excess, cell parameters and cell volume evolutions observed in our samples at $y_{123} = 0.04$, i.e. just after the iron induced twin-tweed transition, as well as the observed iron-clusters in the CuO chains plane, support the picture of iron substituted at the Cu(1) site and its CuO basal plane disorder effect induced on the charge transfer and T_c [38].

5. Conclusion

The solubility limit of zinc and iron in YBaCuO have been found to be equal to 7 and 19 at %, respectively.

Densification appears to be independent of zinc and iron concentration while both dopants induce grain-growth inhibition with respect to the undoped material. This last phenomenon can be correlated either with segregation at the grain interfaces or with clustering (in the case of iron-doped samples).

The oxygen stoichiometry decrease with increasing zinc concentration and increase with increasing iron concentration, have been interpreted in terms of the charge balance resulting from the dopant charge and copper charge evolution with doping.

The T_c depression on zinc-doping is correlated with the copper charge excess evolution with doping. For $0.0 \leqslant y_{123} < 0.04$, the sharp T_c drop has been interpreted as a pair-breaking effect of zinc substituted in the planes.

Additionally, for $y_{123} > 0.054$, the chain length becomes smaller than the critical length for efficient chain-to-plane charge transfer to occur, and T_c, which shows a plateau-like behaviour for $0.04 \leqslant y_{123} \leqslant 0.054$, falls again sharply following carrier localization on the chain copper ions.

Iron which substitutes for copper in the chains induces a discontinuity in the structure and copper charge excess evolution as a function of iron concentration at a 4 at % iron concentration. This phenomenon can be linked to the twin–tweed structural transition, the consequence of which is a diminution of the chain length with increasing iron concentration, detrimental to the charge transfer and T_c when the iron concentration exceeds 8 at %.

Acknowledgements

This work was supported by "l'Institut pour l'encouragement de la Recherche Scientifique dans l'Industrie et l'Agriculture" (IRSIA) and "le Service pour la Programmation de la Politique Scientifique" (SPPS), under contract number SU02/009. The authors thank Mrs M. Deweerdt and Mr G. Schmitz for useful help in iodometric titration measurements.

References

1. T. R. CHIEN, Z. Z. WANG and N. P. ONG, *Phys. Rev. Lett.* **67** (1991) 2088.
2. P. H. ANDRESEN, H. FJELLVAG, P. KAREN and A. KJEKSHUS, *Acta Chem. Scand.* **45** (1991) 698.
3. R. LIANG, T. NAKAMURA, H. KAWAJI, M. ITOH and T. NAKAMURA, *Phys. C* **170** (1990) 307.
4. P. P. PARSHIN, V. P. GLAZKOV, M. G. ZEMLYANOV, A. V. IRODOVA, O. E. PARFENOV and A. A. CHERNYSHEV, *Superconductivity* **5** (1992) 445.
5. H. SHIMIZU, T. KIYAMA and J. ARAI, *Phys. C* **196** (1992) 329.
6. Y. XU, R. L. SABATINI, A. R. MOODENBAUGH, Y. ZHU, S.-G. SHYU, M. SUENAGA, K. W. DENNIS and R. W. McCALLUM, *ibid.* **169** (1990) 205.
7. J. M. TARASCON, P. BARBOUX, P. F. MICELI, L. H. GREENE, G. W. HULL, M. ELIBSCHUTZ and S. A. SUNSHINE, *Phys. Rev. B* **37** (1988) 7458.
8. M. MEHBOD, W. BIBERACHER, A. G. M. JANSEN, P. WYDER, R. DELTOUR and P. H. DUVIGNEAUD, *ibid.* **38** (1988) 11813.
9. Y. XU, M. SUENAGA, J. TAFTO, R. L. SABATINI, A. R. MOODENBAUGH and P. ZOLLIKER, *ibid.* **39** (1989) 6667.
10. M. MEHBOD, P. WYDER, R. DELTOUR, P. H. DUVIGNEAUD and G. NAESSENS, *ibid.* **36** (1987) 8819.
11. E. BAGGIO-SAITOVITCH, *Hyperfine Interact.* **66** (1991) 231.
12. V. MARQUINA, M. L. MARQUINA, M. JIMENEZ, S. ABURTO, R. GOMEZ and R. ESCUDERO, *ibid.* **66** (1991) 423.
13. E. BAGGIO-SAITOVITCH, R. B. SCORZELLI, I. SOUZA AZEVEDO and C. A. DOS SANTOS, *Solid State Commun.* **74** (1990) 24.
14. G. ROTH, G. HEGER, B. RENKER, J. PANNETIER, V. CAIGNAERT, M. HERVIEU and B. RAVEAU, *Z. Phys. B Condens. Matter* **71** (1988) 43.
15. G. KALLIAS, V. PSYHARIS, D. NAIRCHOS and M. PISSAS, *Phys. C* **174** (1991) 316.
16. I. E. GRABOY, A. R. KAUL, YU D. TRETYAKOV, I. V. ZUBOV and I. G. MUTTIK, *ibid.* **185–189** (1991) 527.
17. T. MIYATAKE, K. YAMAGUCHI, T. TAKATA, N. KOSHIZUKA and S. TANAKA, *Phys. Rev. B* **44** (1991) 10139.
18. G. BALAKRISHNAN, L. W. J. CAVES, R. DUPREE, D. McK. PAUL and M. E. SMITH, *Phys. C* **161** (1989) 9–12.
19. H. YAMAGATA, K. INADA and M. MATSUMURA, *ibid.* **185–189** (1991) 1101.

20. K. WESTERHOLT, H. J. WÜLLER, H. BACH and P. STAUCHE, *Phys. Rev. B* **39** (1989) 11680.
21. H. ALLOUL, T. OHNO, H. CASALTA, J. F. MARUCCO, P. MENDELS, J. ARABSKI, G. COLLIN and M. MEHBOD, *Phys. C* **171** (1991) 419.
22. P. WEI and Z. QING QI, *ibid.* **183** (1991) 32.
23. J. L. GARCIA-MUNOZ, X. OBRADORS, S. H. KILCOYNE and R. CYWINSKI, *ibid.* **185–189** (1991) 1085.
24. V. A. TROUNOV, T. YU KAGANOVICH, A. I. KURBAKOV, A. V. MATVEEV, A. M. BALAGUROV, A. W. HEWAT, P. FISCHER, O. ANTSON and R. M. A. MAAYOUF, *ibid.* **197** (1992) 123.
25. A. KULPA, A. C. D. CHAKLADER and G. ROEMER, *ibid.* **191** (1992) 282.
26. T. INABA, Y. TAKANO and K. SEKIZAWA, *Solid State Commun.* **70** (1989) 725.
27. T. KREKELS, private communication (1993).
28. B. ULLMANN, R. WORDENWEBER, K. HEINEMANN, H. U. KREBS, H. C. FREYHARDT and E. SCHWARZMANN, *Phys. C* **153–155** (1988) 871.
29. T. KREKELS, G. VAN TENDELOO, D. BRODDIN, S. AMELINCKX, L. TANNER, M. MEHBOD, E. VANLATHEM and R. DELTOUR, *ibid.* **173** (1991) 361.
30. P. BORDET, J. L. HODEAU, P. STROBEL, M. MAREZIO and A. SANTORO, *Solid State Commun.* **66** (1988) 435.
31. R. M. GERMAN, in "Engineered materials handbook (Vol. 4): Ceramics and Glasses", volume chairman S. J. Schneider Jr (ASM International, Metals Park, OH, USA, 1991), p. 260.
32. M. MAREZIO, *Acta Crystallogr A* **47** (1991) 640.
33. J. D. JORGENSEN, D. G. HINKS, P. G. RADAELLI, S. PEI, P. LIGHTFOOT, B. DABROWSKI, C. U. SEGRE and B. A. HUNTER, *Phys. C* **185–189** (1991) 184.
34. X. MING, L. ZHENG-ZHONG and S. DA-NING, *ibid.* **202** (1992) 363.
35. A. LANCKBEEN, C. LEGROS, J. F. MARUCCO, R. DELTOUR, *ibid.* Physica C. **221** (1994) 53.
36. T. KAJITANI, K. KUSABA, M. KIKUCHI, Y. SYONO and M. HIRABAYASHI, *J. Appl. Phys.* **27** (1988) L-354.
37. G. ROTH, P. ADELMANN, R. AHRENS, B. BLANK, H. BÜRKLE, F. GOMPF, G. HEGER, M. HERVIEU, M. NINDEL, B. OBST, J. PANNETIER, B. RAVEAU, B. RENKER, H. RIETSCHEL, B. RUDOLF and H. WÜHL, *Phys. C* **162–164** (1989) 518.
38. C. Y. YANG, A. R. MOODENBAUGH, Y. L. WANG, Y. XU, S. M. HEALD, D. O. WELCH, M. SUENAGA, D. A. FISCHER and J. E. PENNER-HAHN, *Phys. Rev. B* **42** (1990) 2231.
39. I. D. BROWN, *J. Solid State Chem.* **90** (1991) 155.
40. J. K. BURDETT, *Phys. C* **191** (1992) 282.

Received 16 April
and accepted 10 December 1993